Supplementary Material (ESI) for PCCP

Supporting Information

Mechanistic Studies of the 'Blue' Cu Enzyme, Bilirubin Oxidase, as a Highly Efficient Electrocatalyst for the Oxygen Reduction Reaction

Luciano dos Santos †‡, Victor Climent §, Christopher F. Blanford †

and Fraser A. Armstrong †*

† Inorganic Chemistry Laboratory, University of Oxford, Oxford, UK; ‡ Instituto de Química de São Carlos, Universidade de São Paulo, São Carlos, Brazil; §Instituto de Electroquímica, Universidad de Alicante, Alicante, Spain.

CONTENTS

- Figure S8. Cyclic voltammograms showing the electrocatalytic reduction of dioxygen by platinum electrodeposited on PGE and by *Mv*BO adsorbed on 6A2NA-modified PGE with their corresponding second derivatives as a function of pH.
- Figure S9: Stability of continually cycled *Mv*BO-coated 6A2NA-modified PGE electrode.
- Figure S10. Sample Koutecký-Levich plot for *Mv*BO on a rotating PGE electrode.
- Figure S11. Replot of Fig. 4C–D showing full current scale.
- Figure S12. Catalytic voltammogram of *Mv*BO on Au(111) electrode and fit to "dispersion" model.
- Table S1. Fitting parameters and goodness-of-fit values for *Mv*BO voltammograms shown in main paper.
- Description of non-linear least-squares fitting procedure applied to current vs $p(O_2)$ data.
- Table S2. Absolute and relative errors in flow rate in K_M and i_{max} determinations.

Enzyme Purification. Bilirubin oxidase (*Mv*BO) from *Myrothecium verrucaria* was purified from the crude powder by applying a suspension (2 mg mL^{-1} in 50 mM Tris-H_2SO_4 buffer at pH 7.6) to a DEAE-Sepharose CL-6B (*ca* 2 mL resin) weak anionic exchange column equilibrated with the same buffer, at 4°C. After washing the enzyme loaded column, the elution was carried out with a linear gradient from 0 to 0.25 M $(NH_4)_2SO_4$ in the same buffer. The blue fractions containing bilirubin oxidase were pooled, combined and dialyzed to a 20 mM acetate buffer (pH 4.5) containing 1.8 M $(NH_4)_2SO_4$ using a PM-30 filter (Amicon) and a yellow band not containing bilirubin oxidase remained in the column. The dialyzed sample was then applied to a HiTrap Phenyl HP hydrophobic column, equilibrated with the same acetate buffer, and the elution was carried out with a linear reverse salt gradient of 1.8 to 0 M $(NH_4)_2SO_4$. The fractions were then pooled and dialyzed against 0.1 M sodium phosphate at pH 7.0, but they were not combined before or after the dialysis. All purified samples were frozen in liquid nitrogen and stored in a –80°C freezer. The use of HCl, NaCl or any other halide was avoided in all steps of purification and also during electrochemical experiments to avoid inhibition.

Activity Assay. The total protein concentration of the stock solutions for both purified and non-purified bilirubin oxidase was calculated using the Beer-Lambert law based on $A_{280\ nm}$ measured from enzyme aliquots and using $\varepsilon_{280\ nm} = 9.52 \times 10^4\ M^{-1}\ cm^{-1}$, calculated from the enzyme amino acid sequence by the online software ProtParam – Expasy Proteomics Server (http://www.expasy.ch/tools/protparam.html).

For the specific activity assay of *Mv*BO toward oxidation of 2,2'-azino-bis(3-ethylbenzthiazoline-6-sulphonic acid) (ABTS), 2 μL of a 50 times diluted stock solution of bilirubin oxidase (providing a concentration of 2–3 nM of total protein into the cuvette solution) was added to 3 mL of 0.1 M sodium phosphate pH 6.0 and 24 °C, containing 30 μM of ABTS, and the absorption at 340 nm was immediately recorded. The enzyme activity was determined from the rate of conversion of $ABTS^{2-}$ to $ABTS^{-\bullet}$ measured by the decrease in absorption at 340 nm with time, based on the reaction rate between 5 and 25 s after mixing, according to Equation S1.

$$\text{Specific activity} = \frac{-\left(\frac{dA}{dt}\right)}{\varepsilon b[\text{E}]} \qquad [S1]$$

where A is the absorbance at 340 nm, t is time in minutes, ε is the molar absorbance of $ABTS^{2-}$ at 340 nm (3.45×10^4 M^{-1} cm^{-1}),[1] b is the cuvette pathlength (1 cm). We define 1 unit of activity (U) as the amount of enzyme which converts 1 µmol of ABTS per minute at pH 6.0 and 24 °C. The measurement was repeated three times for both purified and 'as-received' bilirubin oxidase. The specific activity of the purified *Mv*BO was 2.49 ± 0.13 U $nmol^{-1}$ (41.4 ± 1.3 kat mol^{-1}) and the value for the non-purified *Mv*BO was 1.63 ± 0.04 U $nmol^{-1}$ (27.2 ± 0.7 kat mol^{-1}). This represents an improvement in activity of (52 ± 16)% upon purification. Using a molecular weight of 64.2 kDa for the protein, the mass specific activity is 38.7 ± 2.0 U mg^{-1} (645 ± 33 mkat mg^{-1}) for the purified enzyme and 25.4 ± 0.7 U mg^{-1} (424 ± 11 mkat mg^{-1}) for the 'as-received' enzyme. Precision given is based on the standard deviation of the slope measurements and standard rules for propagation of error.

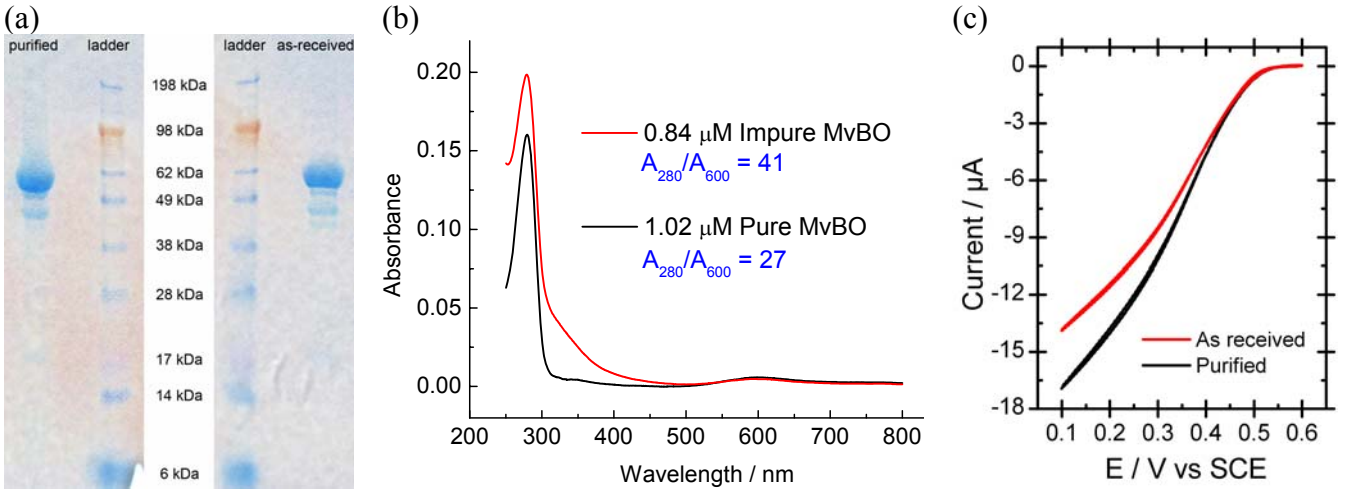

Figure S1: (a) SDS-PAGE for the purified and as-received *Mv*BO reduced by boiling with 2-mercaptoethanol. (b) UV/Vis spectra for the *Mv*BO before and after the purification. Conditions: 0.1 M sodium phosphate, pH 5.0, 25 °C. (c) Comparison of electrocatalytic oxygen reduction performance of as-received and purified *Mv*BO on identically treated, 6A2NA-modified PGE electrodes. Conditions: 0 °C, 0.1 M sodium phosphate pH 6.0, 2500 rpm, 1 bar O_2.

[1] *Journal of Electroanalytical Chemistry* 1999, **464**, 110–117.

Construction of the PGE electrode. Pyrolytic graphite plates (Momentive Performance Materials Inc., Strongsville, Ohio, USA) were cut into strips (3 mm × 3 mm × 5 cm) and machined into 2-mm-diameter cylinders, in such a way that the edge plane of the plate comprised the end faces of the rod with a geometric surface area of 0.03 cm^2. The electrical connection was made with a silver-loaded two-part epoxy (RS Inc., Corby, UK) between the graphite and a stainless steel rod, which was embedded into a nylon cylinder. The graphite rod was embedded in epoxy resin (CY1300 and HY1300, Robnor Resins, Swindon, UK) and cured overnight. Fresh circular cross-sections of the embedded graphite were exposed by abrading the electrode tip with Norton Tufbak P400 silicon carbide waterproof abrasive paper (RS).

Comparisons of electrocatalytic waveforms in H_2O vs D_2O. Each measurement was made using successive transfers between H_2O and D_2O buffer solutions The 6A2NA-*Mv*BO modified PGE electrode was placed in O_2-saturated H_2O buffer at the desired pH, three scans of cyclic voltammetry were recorded at 5 mV s^{-1}, and the electrode was transferred to an O_2-saturated D_2O buffer at the equivalent pD. Three scans were then recorded, in exactly the same way, and the electrode was returned to the H_2O buffer solution, repeating the process in a second series. This procedure was carried out at each pL unit between 5.0 and 9.0.

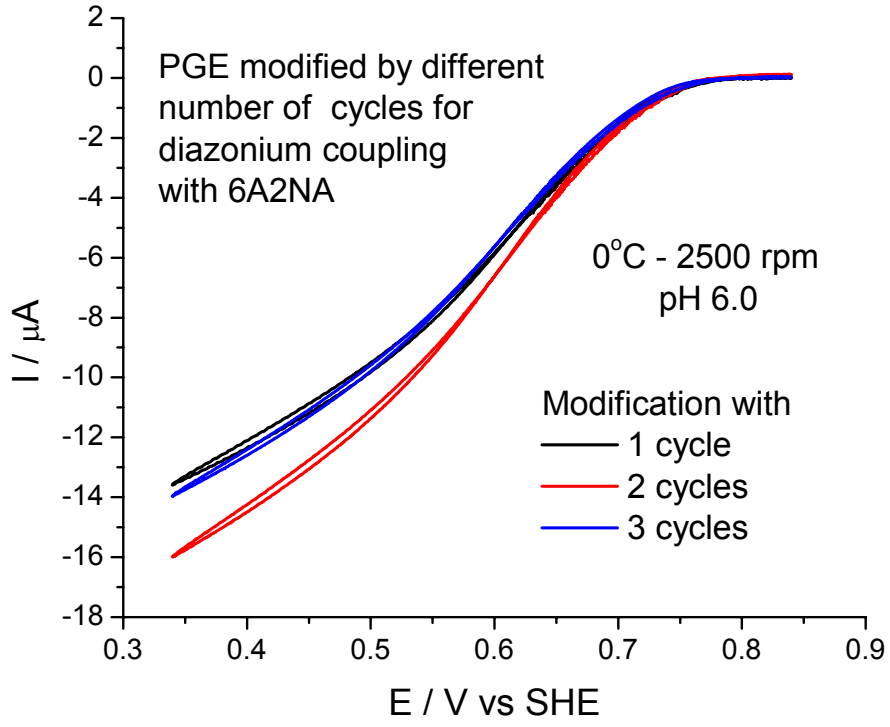

Figure S2: Comparison among the oxygen reduction reactions catalysed by *Mv*BO attached to a PGE surface modified with 6-amino-2-naphthoic acid. Number of cycles indicated by the legend refers to the number of potential cycles while the bare, freshly polished electrode was in the 6-diazo-2-naphthoic acid modification solution, rather than the number of cycles in oxygenated buffer. Conditions: pH 6.0, 0.1 M sodium phosphate, 5 mV s^{-1}, 0 °C, 2500 rpm, 1 bar O_2, first CV cycle shown.

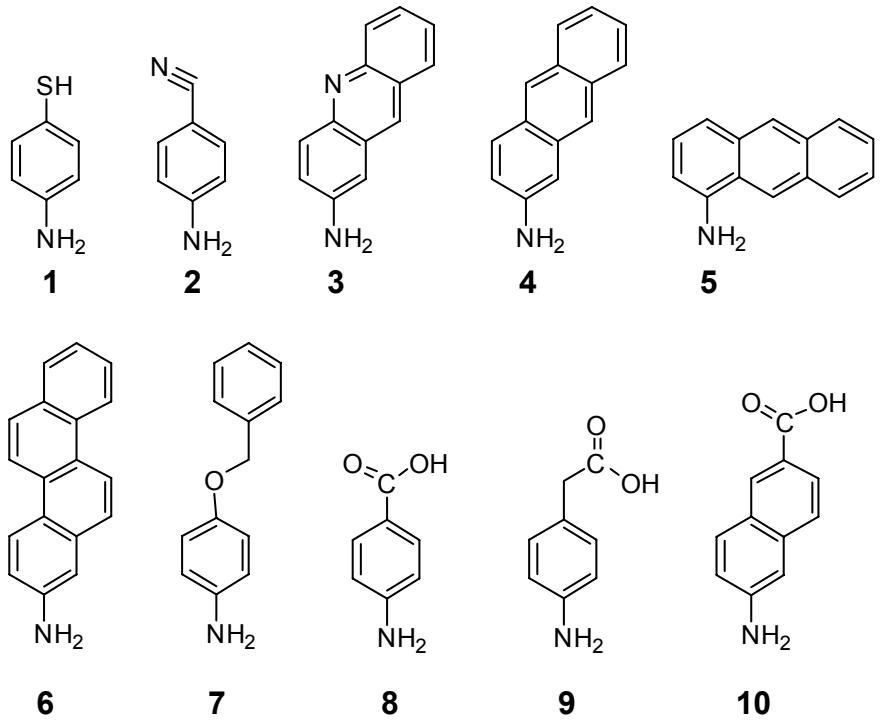

Figure S3: Representation of the structures of the molecules tested as modifiers for the graphite surface to enhance the binding of *Mv*BO. (**1**) 4-aminothiophenol; (**2**) 4-aminobenzonitrile; (**3**) 2-aminoacridine; (**4**) 2-aminoanthracene; (**5**) 1-aminoanthracene; (**6**) 2-aminochrysene; (**7**) 4-benzyloxyaniline; (**8**) 4-aminobenzoic acid; (**9**) 4-aminophenylacetic acid; (**10**) 6-amino-2-naphthoic acid.

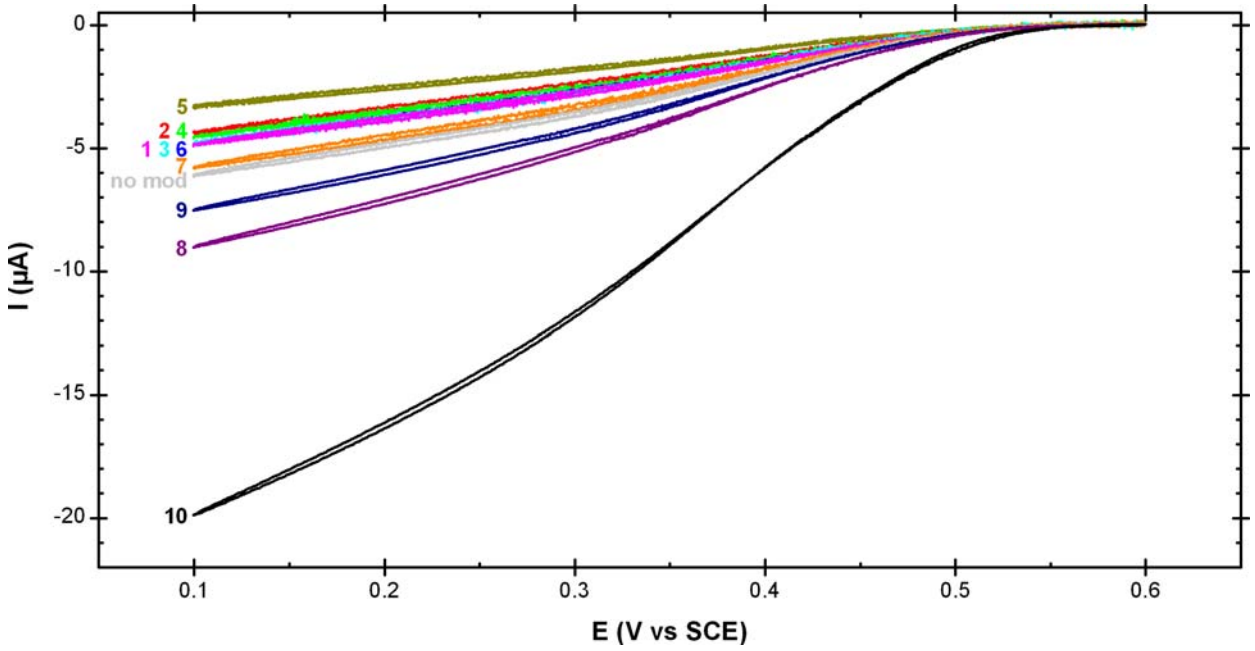

Figure S4: Comparison of the efficiency of O_2 reduction catalysed by *Mv*BO adsorbed on unmodified PGE and PGE modified by the diazotized form of the molecules shown in Fig. S3. Conditions: 0.1 M sodium phosphate, pH 5.5, 5 mV s^{-1}, 0 °C, 2500 rpm, 1 bar O_2.

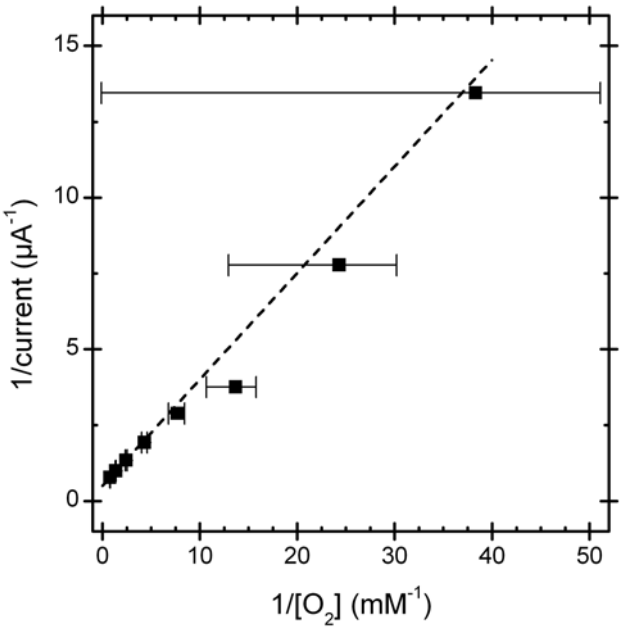

Figure S5: Lineweaver-Burk (double-reciprocal) plots for the O_2 reduction reaction catalysed by *Mv*BO immobilized on a 6A2NA-modified PGE electrode, depicting the linear relationship between the reciprocal current (proportional to reciprocal reaction velocity) and the reciprocal of the oxygen concentration in solution. Conditions: 0.1 V vs SCE, 0.1 M sodium phosphate, pH 5.0, 25 °C, 3500 rpm.

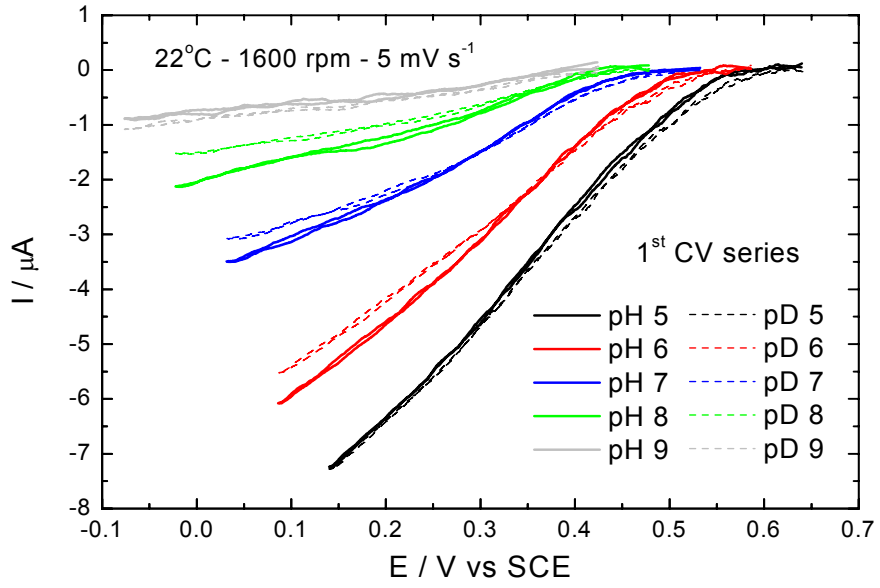

Figure S6: Cyclic voltammograms showing the effect of different pL values (L = H, D) on the reduction of dioxygen catalysed by *Mv*BO immobilized on a 6A2NA-modified PGE electrode, obtained during successive transfers between H_2O and D_2O buffer solutions. The enzyme-coated electrode was immersed into H_2O buffer at a given pH, three cycles were recorded, then the electrode was transferred (after removing excess electrolyte) to the D_2O buffer at the equivalent pD where three cycles were also recorded. Each pair of measurements was recorded twice for each pL value. Buffer: 2.85 mM $Na_2B_4O_7{\cdot}10H_2O$ (sodium tetraborate), 10.0 mM $Na_2HPO_4{\cdot}7H_2O$ (sodium phosphate dibasic heptahydrate) and 6.70 mM $Na_3C_6H_5O_7$ (sodium citrate). The desired pL was adjusted by adding NaOH or NaOD and H_2SO_4 or D_2SO_4. To calculate pD values, 0.4 units were added to the value reported by the proton-sensitive pH probe calibrated in buffered H_2O. Conditions: 5 mV s^{-1}, 22°C, 1600 rpm, 1 bar O_2.

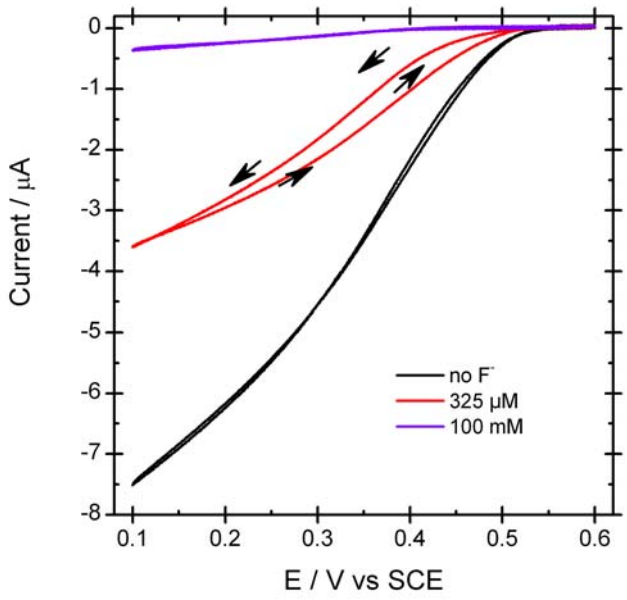

Figure S7. Fluoride inhibition of oxygen reduction catalysis from *Mv*BO on 6A2NA-modified PGE. Direction arrows in the 325 µM trace highlight the hysteresis in the inhibited catalytic response. Conditions: 0.1 M sodium phosphate, 25 °C, 5 mV s^{-1}, 2500 rpm, 1 bar O_2, cycle 1 shown.

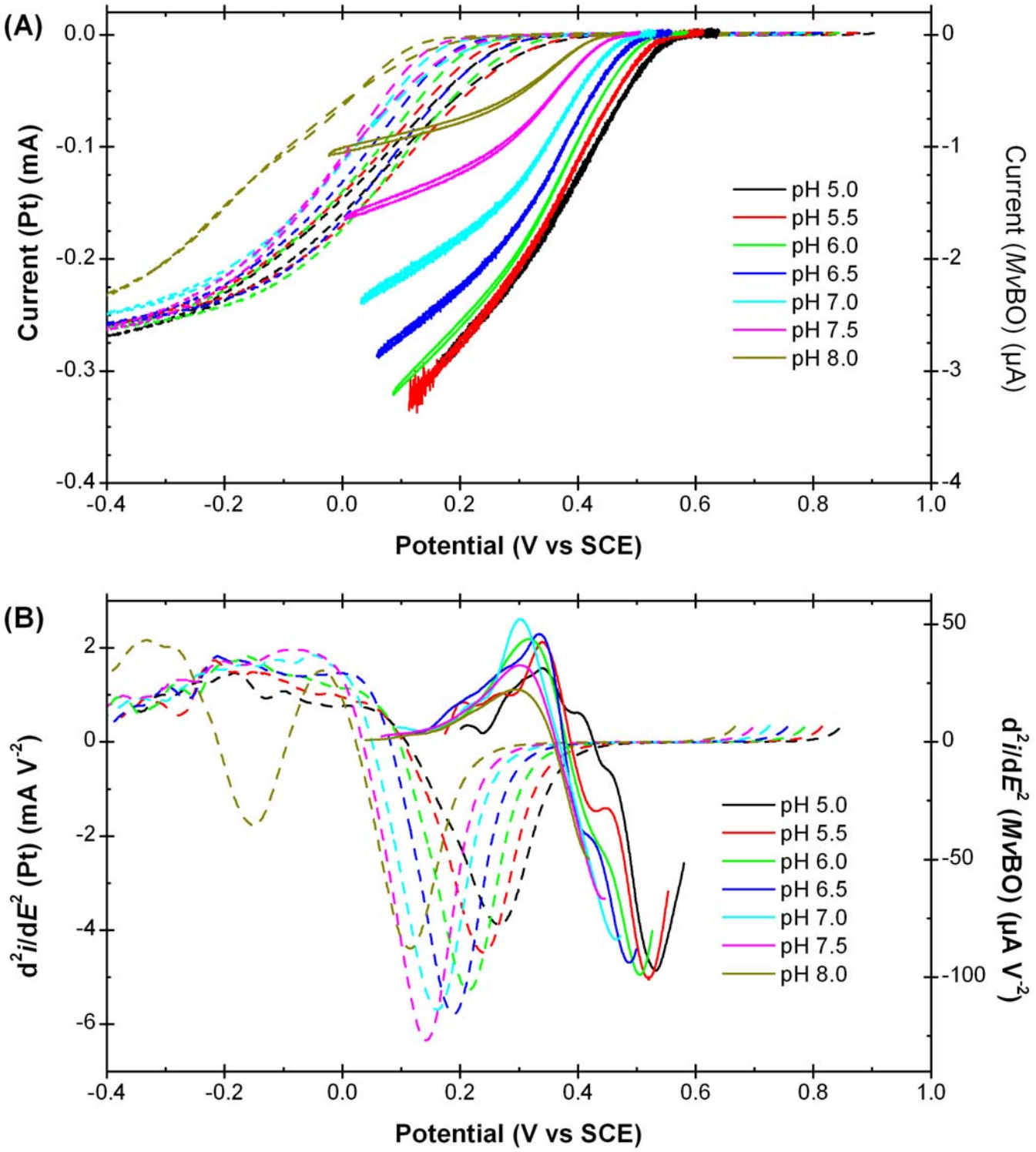

Figure S8. (A) Cyclic voltammograms showing the electrocatalytic reduction of dioxygen by platinum electrodeposited on PGE and by *Mv*BO adsorbed on 6A2NA-modified PGE with (B) their corresponding second derivatives as a function of pH. The platinum data are shown as dashed lines and refer to the left axis; bilirubin oxidase data are shown as solid lines and refer to the right axis. Conditions: 0.1 M sodium phosphate, 0 °C, 5 mV s^{-1}, 2500 rpm, 1 bar O_2, cycle 3 shown.

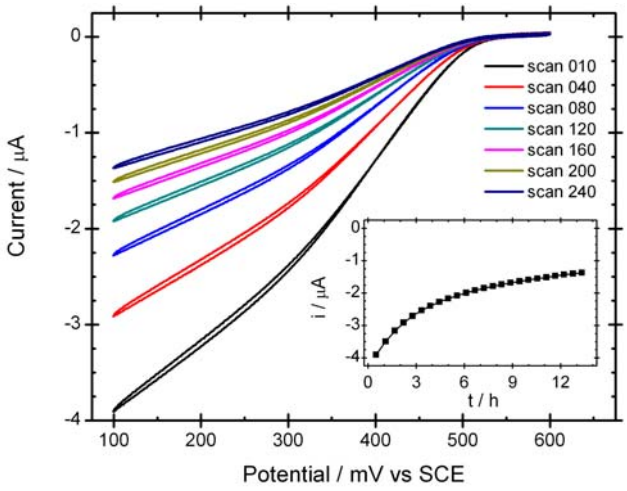

Figure S9. Stability of continually cycled *Mv*BO-coated 6A2NA-modified PGE electrode. *Main frame:* Seven of the 240 electrocatalytic waves recorded. *Inset:* Change in activity with time as illustrated by the catalytic current at 0.1 V vs SCE on every 10th cycle. Electrode was modified and stored for 3 d as described in Experimental. Conditions: 3 mm^2, 2500 rpm, 1 bar O_2, 25 °C, 0.1 M sodium phosphate pH 6.0 (presaturated with O_2 for 30 minutes before scanning), 5 mV s^{-1}.

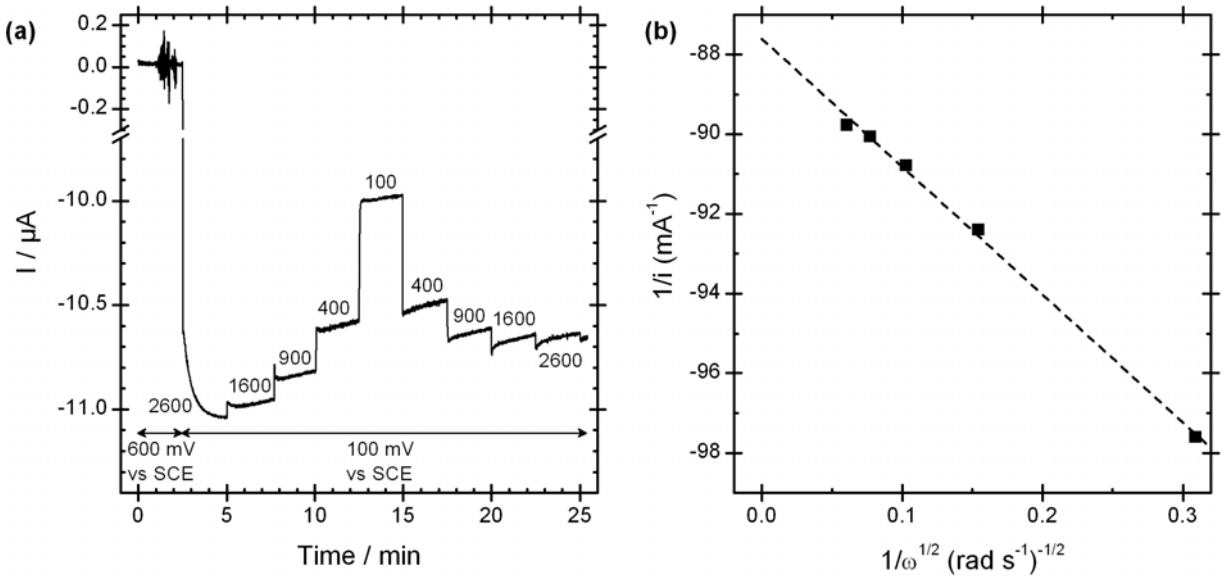

Figure S10. Sample Koutecký-Levich plot for MvBO on a rotating PGE electrode. (a) Electrocatalytic chronoamperometric trace of *Mv*BO on 6A2NA-modified PGE electrode. Numbers beside the trace denote rotation rate in rpm. (b) Linearized plot of current vs rotation rate data. Extrapolated current magnitude at infinite rotation rate is 2.2% higher than that at 2500 rpm. Conditions: 3 mm^2, 0.1 M sodium phosphate pH 6.0, 25 °C, 1 bar O_2.

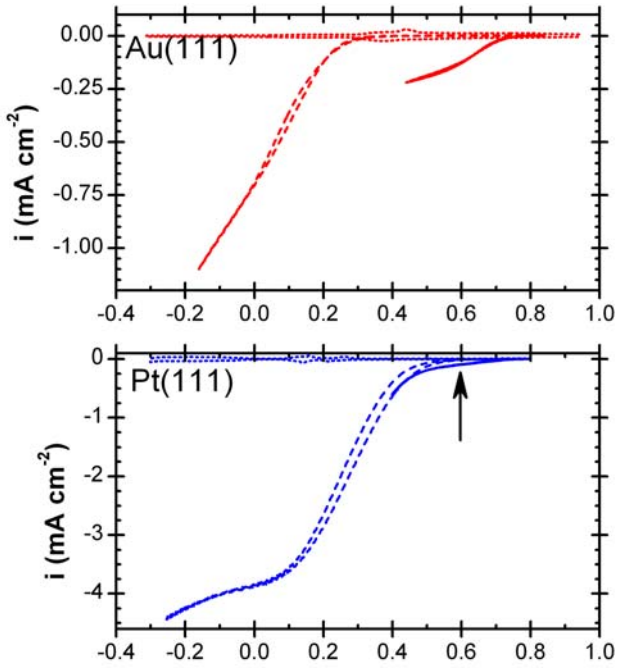

Figure S11. Replot of Fig. 4C–D showing full current scale. Conditions as in Fig. 4C-D.

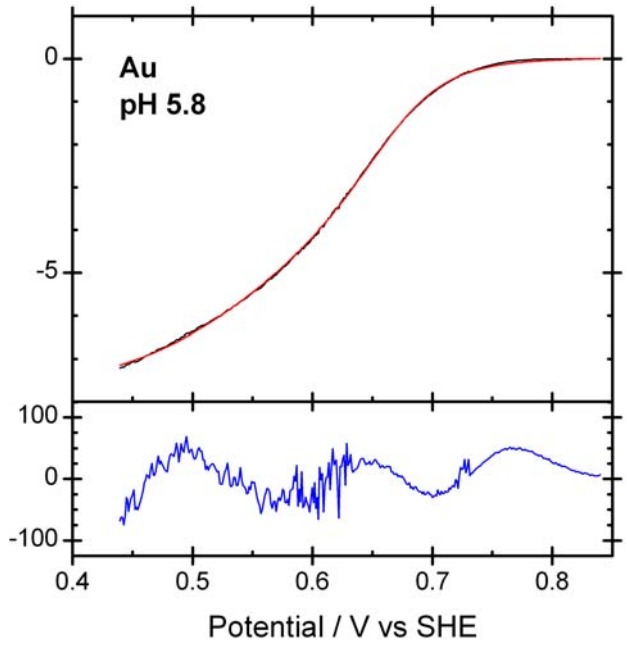

Figure S12. Catalytic voltammogram of *Mv*BO on Au(111) electrode and fit to "dispersion" model. Conditions the same as in Fig. 4C.

Table S1. Fitting parameters and goodness-of-fit values for *Mv*BO voltammograms shown in main paper.

pH	*T* / °C	E_{cat} / V vs SHE	$\log(k_{cat}/k_0^{max})$	β d_0	i_{lim} / μA	χ^2
5.0	0	0.724	–0.621	8.31	–3.16	6.32×10^{-4}
5.0	0	0.723	–0.686	8.51	–3.24	8.21×10^{-4}
5.5	0	0.714	–0.612	8.11	–3.49	1.06×10^{-3}
6.0	0	0.682	–0.869	8.24	–3.09	1.08×10^{-3}
6.5	0	0.668	–1.030	8.57	–2.95	1.30×10^{-3}
7.0	0	0.630	–1.810	8.86	–1.37	4.81×10^{-4}
7.5	0	0.622	–1.862	9.78	–1.24	2.26×10^{-4}
8.0	0	0.605	–2.202	9.87	–0.68	6.98×10^{-5}
6.0	0	0.670	–0.695	8.40	–1.44	9.84×10^{-5}
6.0	5	0.672	–0.713	8.30	–1.90	1.77×10^{-4}
6.0	10	0.662	–0.906	8.89	–2.19	2.86×10^{-4}
6.0	15	0.670	–0.787	8.20	–2.68	3.22×10^{-4}
6.0	20	0.674	–0.809	8.20	–3.20	4.26×10^{-4}
6.0	25	0.674	–0.886	8.25	–3.59	5.30×10^{-4}
6.0	30	0.672	–0.992	8.32	–3.87	6.13×10^{-4}
6.0	35	0.668	–1.167	8.59	–3.73	6.57×10^{-4}
6.0	40	0.673	–1.194	8.69	–3.62	4.50×10^{-4}
5.8	*20*	0.661	–1.012	6.02	–0.23	8.84×10^{-8}

1. Italics indicate Au(111) surface.
2. Fits based on reductive sweep.
3. A linear baseline was fit to the voltammogram at a point before the onset of catalysis and incorporated in this model.
4. $\chi^2 = \frac{\Sigma(i_{fit}-i_{meas})}{n}$ where the summation is over the potential range fit and n is the number of current measurements in that range

Description of non-linear least-squares fitting procedure applied to current vs $p(O_2)$ data.

Although the data are presented as double-reciprocal (Lineweaver-Burk plots), the fit to the data was performed by a non-linear least-squares procedure in which the minimized variable, χ^2, was weighted by the relative error in the gas concentration (Equation [S2]). Here, we solved the Michaelis-Menten equation for the substrate concentration (Equation [S3]) which was assumed to have a greater and more significant uncertainty than our current measurement had. The relative errors in the substrate and balance gas were based on published uncertainties from the suppliers of the mass flow controllers (1% of full scale; here either 10 sccm or 25 sccm) (Equation [S4]). Although the rearragement in equation [S3] swaps the dependent and independent variables to allow the uncertainty in the gas concentration to weight the residual minimization, both the variables remain independent of each other. This method contrasts with analysis by Hanes-Woolf (S/v vs S) and Eadie-Hofstee (v vs v/S) plots in which the ordinate or abscissa on the plot is a ratio of the two variables.

$$\chi^2 = \sum \left(\frac{S_{\text{fit}} - S_{\text{meas}}}{(\sigma_S / S_{\text{meas}})} \right)^2 \qquad [S1]$$

$$S = \frac{v\, K_M}{V_{\max} - v} \qquad [S2]$$

$$\left(\frac{\sigma_S}{S_{\text{meas}}} \right) = \sqrt{\left(\frac{\sigma_S}{S_{\text{meas}}} \right)^2 + \left(\frac{\sqrt{\sigma_S + \sigma_X}}{S + X} \right)^2} \qquad [S3]$$

where S and X the concentrations of the substrate and balance gas, respectively (here $[O_2]$ and [Ar], both assumed to be proportional to their relative flow rates; their Henry's law constants differ by <10%); v and $V_{\max}$ are the measured and (extrapolated) maximum reaction rates, respectively (both proportional to current), σ is the absolute error in the concentration measurement, and χ^2 is our minimization parameter. Values of S, X and σ_S for a typical run are shown in Table S2.

Table S2. Absolute and relative errors in flow rate in K_M and i_{max} determinations.

Ar / sccm [a]	O_2 / sccm [b]	fraction O_2	$[O_2]$ / mM	$\sigma_{[O2]}$ / mM	$\sigma_{[O2]}/[O_2]$
0	996	100.0%	1.300	0.037	2.9%
436	560	56.2%	0.731	0.024	3.2%
681	315	31.6%	0.411	0.017	4.2%
819	177	17.8%	0.231	0.014	6.3%
896	100	10.0%	0.130	0.014	10.4%
940	56	5.6%	0.073	0.013	18.1%
965	31	3.2%	0.041	0.013	31.9%
976	20	2.0%	0.026	0.013	50.1%

[a] 25 sccm uncertainty
[b] 10 sccm uncertainty